Reply to Comment on Breakdown of Colloid Filtration Theory: Role of the Secondary Energy Minimum and Surface Charge Heterogeneities

ARTICLE *in* LANGMUIR · MARCH 2005

Impact Factor: 4.46 · DOI: 10.1021/la048102g · Source: PubMed

2 AUTHORS:

Nathalie Tufenkji
McGill University
122 PUBLICATIONS **3,629** CITATIONS

SEE PROFILE

Menachem Elimelech
Yale University
395 PUBLICATIONS **32,645** CITATIONS

SEE PROFILE

Breakdown of Colloid Filtration Theory: Role of the Secondary Energy Minimum and Surface Charge Heterogeneities

Nathalie Tufenkji*,† and Menachem Elimelech‡

Department of Chemical Engineering, McGill University, Montreal, Quebec H3A 2B2, Canada, and Department of Chemical Engineering, Environmental Engineering Program, P.O. Box 208286, Yale University, New Haven, Connecticut 06520-8286

Received July 27, 2004. In Final Form: November 15, 2004

The mechanisms and causes of deviation from the classical colloid filtration theory (CFT) in the presence of repulsive Derjaguin−Landau−Verwey−Overbeek (DLVO) interactions were investigated. The deposition behavior of uniform polystyrene latex colloids in columns packed with spherical soda-lime glass beads was systematically examined over a broad range of physicochemical conditions, whereby both the fluid-phase effluent particle concentration and the profile of retained particles were measured. Experiments conducted with three different-sized particles in a simple (1:1) electrolyte solution reveal the controlling influence of secondary minimum deposition on the deviation from CFT. In a second series of experiments, sodium dodecyl sulfate (SDS) was added to the background electrolyte solution with the intent of masking near-neutrally charged regions of particle and collector surfaces. These results indicate that the addition of a small amount of anionic surfactant is sufficient to reduce the influence of certain surface charge inhomogeneities on the deviation from CFT. To verify the validity of CFT in the absence of surface charge heterogeneities, a third set of experiments was conducted using solutions of high pH to mask the influence of metal oxide impurities on glass bead surfaces. The results demonstrate that both secondary minimum deposition and surface charge heterogeneities contribute significantly to the deviation from CFT generally observed in colloid deposition studies. It is further shown that agreement with CFT is obtained even in the presence of an energy barrier (i.e., repulsive colloidal interactions), suggesting that it is not the general existence of repulsive conditions which causes deviation but rather the combined occurrence of "fast" and "slow" particle deposition.

1. Introduction

Prediction of particle deposition behavior in saturated porous media is of practical interest in a number of engineering applications. Examples include chromatographic separation,[1] granular (deep-bed) filtration in water and wastewater treatment,[2,3] transport and fate of colloids and colloid-associated pollutants in the subsurface environment,[4−6] and natural filtration of microorganisms such as bacteria, viruses, and protozoa.[7−9]

The most commonly used approach for describing filtration of colloidal particles, generally referred to as the classical colloid filtration theory (CFT), was originally developed by Yao et al.[10] In this classic "clean-bed" filtration model, the removal of suspended particles is represented by first-order kinetics, resulting in concentrations of suspended and retained particles that decline exponentially with distance. Despite widespread use in modeling and experimental studies, a growing body of evidence suggests that the deposition behavior of microbial particles (e.g., bacteria and viruses) is inconsistent with the classical CFT.[11−17] Such observations of microbial deposition that diverge significantly from predictions based on CFT have important implications for numerous processes in natural and engineered systems. Particularly, these results suggest that predictions of particle removal in saturated porous media are considerably overestimated by the classical CFT. Several explanations have been proposed to account for this observed deviation from CFT, including heterogeneity in microbial surface properties,[12,17] distributions in the interaction energies between particles and collector grains,[18,19] and particle deposition dynamics.[18] Although the causes of deviation from CFT with respect to filtration of microbial particles have been

* Corresponding author: phone, (514) 398-2999; fax, (514) 398-6678; e-mail, nathalie.tufenkji@mcgill.ca.
† McGill University.
‡ Yale University.

(1) Prieve, D. C.; Hoysan, P. M. *J. Colloid Interface Sci.* **1978**, *64*, 201−213.
(2) Tobiason, J. E.; O'Melia, C. R. *J. Am. Water Works Assoc.* **1988**, *80*, 54−64.
(3) Tien, C.; Payatakes, A. C. *AIChE J.* **1979**, *25*, 737−759.
(4) McDowell-Boyer, L. M.; Hunt, J. R.; Sitar, N. *Water Resour. Res.* **1986**, *22*, 1901−1921.
(5) McCarthy, J. F.; Zachara, J. M. *Environ. Sci. Technol.* **1989**, *23*, 496−502.
(6) Ryan, J. N.; Elimelech, M. *Colloid Surf., A* **1996**, *107*, 1−56.
(7) Harvey, R. W.; Garabedian, S. P. *Environ. Sci. Technol.* **1991**, *25*, 178−185.
(8) Schijven, J.; de Bruin, H. A. M.; Hassanizadeh, S. M.; Husman, A. M. D. *Water Res.* **2003**, *37*, 2186−2194.
(9) Tufenkji, N.; Ryan, J. N.; Elimelech, M. *Environ. Sci. Technol.* **2002**, *36*, 422a−428a.
(10) Yao, K. M.; Habibian, M. T.; O'Melia, C. R. *Environ. Sci. Technol.* **1971**, *5*, 1105−1112.
(11) Albinger, O.; Biesemeyer, B. K.; Arnold, R. G.; Logan, B. E. *Fems Microbiol. Lett.* **1994**, *124*, 321−326.
(12) Baygents, J. C.; Glynn, J. R.; Albinger, O.; Biesemeyer, B. K.; Ogden, K. L.; Arnold, R. G. *Environ. Sci. Technol.* **1998**, *32*, 1596−1603.
(13) Bolster, C. H.; Mills, A. L.; Hornberger, G. M.; Herman, J. S. *Water Resour. Res.* **1999**, *35*, 1797−1807.
(14) Camesano, T. A.; Logan, B. E. *Environ. Sci. Technol.* **1998**, *32*, 1699−1708.
(15) Martin, M. J.; Logan, B. E.; Johnson, W. P.; Jewett, D. G.; Arnold, R. G. *J. Environ. Eng.-ASCE* **1996**, *122*, 407−415.
(16) Redman, J. A.; Estes, M. K.; Grant, S. B. *Colloid Surf., A* **2001**, *191*, 57−70.
(17) Simoni, S. F.; Harms, H.; Bosma, T. N. P.; Zehnder, A. J. B. *Environ. Sci. Technol.* **1998**, *32*, 2100−2105.
(18) Tufenkji, N.; Redman, J. A.; Elimelech, M. *Environ. Sci. Technol.* **2003**, *37*, 616−623.
(19) Li, X.; Scheibe, T. D.; Johnson, W. P. *Environ. Sci. Technol.* **2004**, *38*, 5616−5625.

10.1021/la048102g CCC: $30.25
Published on Web 01/07/2005

hypothesized, the mechanisms controlling this behavior have not been fully elucidated.

Tufenkji and Elimelech[20] have recently verified the validity of the classical CFT using a well-controlled experimental system where they examined the deposition behavior of uniform polystyrene microspheres in columns packed with glass bead collectors. The results of their experimental and theoretical investigation indicate that even under well-controlled model conditions, the concurrent existence of both *favorable* and *unfavorable* chemical−colloidal interactions may cause significant deviation from CFT. Particle deposition is termed *favorable* in the absence of repulsive interaction energies, whereas *unfavorable* deposition refers to the case where repulsive colloidal interactions predominate.[21] To explain their findings, Tufenkji and Elimelech[20] proposed that a fraction of the particle population exhibits "slow" deposition whereby particles with sufficient energy to overcome the repulsive energy barrier can reach the primary energy minimum. The remaining particles deposit at a "fast" rate which is attributed to the presence of a deep secondary energy minimum and surface charge heterogeneities on particle or collector surfaces.

The important role of surface charge heterogeneity in the kinetics of particle deposition[22−24] and coagulation[25,26] under *unfavorable* chemical conditions has been noted for some time. Hull and Kitchener,[22] Bowen and Epstein,[23] and Gregory and Wishart[24] reported the results of controlled colloid deposition experiments under *unfavorable* chemical conditions. They observed that experimental particle deposition rates were many orders of magnitude greater than theoretical predictions based on classic DLVO theory.[27,28] The discrepancy was attributed to inherent physical and chemical/charge heterogeneities of collector surfaces. These investigators further suggested that particle deposition occurs preferentially onto energetically *favorable* sites, resulting in initial deposition rates much higher than those predicted based on the average collector surface potential.

Potential sources of collector surface charge heterogeneity commonly evoked in column deposition studies include near-neutrally charged hydrophobic regions, metal oxide impurities (e.g., Al_2O_3 and Fe_2O_3), and surface-bound contaminants (e.g., organic molecules).[29−31] In a study of colloid deposition in packed beds, Litton and Olson[30] demonstrated how cleaning methods of various silica collector surfaces can significantly influence the rate of particle deposition when *unfavorable* conditions prevail. These investigators also showed how anionic surfactants (e.g., sodium dodecyl sulfate) can be used to mask uncharged or slightly positively charged regions of particle and/or collector surfaces which may provide *favorable* sites for colloid deposition.[29]

Song et al.[31] developed a general theoretical approach for the calculation of colloid deposition rate onto heterogeneously charged surfaces. They showed that minor degrees of charge heterogeneity on collector surfaces can result in particle deposition rates that are orders of magnitude larger than those obtained on similar surfaces having no charge heterogeneity. Additional experimental investigations further emphasize how colloid deposition kinetics are controlled by the degree of patchwise chemical heterogeneity rather than its spatial distribution or average zeta (surface) potential.[32,33]

Although the role of the secondary energy well in colloid deposition has been argued,[34−36] recent experimental and theoretical evidence[37−41] suggests that deposition in the secondary minimum can be a controlling factor of particle deposition kinetics in saturated porous media. Hahn and O'Melia[40] showed how a simple Maxwell model based on deposition into and reentrainment from secondary minima provided more accurate predictions of particle deposition rates than commonly used theoretical approaches for particle deposition in the presence of repulsive energy barriers.[42−44] The latter approaches, such as the interaction force boundary layer model,[42,45] are based on the concept of transport over an energy barrier into the primary minimum and do not consider deposition into the secondary energy well. This type of attachment is considered irreversible due to the very large energy barrier to release from the primary energy minimum. In contrast, it has been proposed that particle deposition in a secondary energy minimum is reversible.[40,41] Moreover, it has been suggested that particles apparently captured in secondary energy wells can be released when this energy well is eliminated following a decrease in solution ionic strength.[37−41,46]

The influence of reversible deposition in a secondary energy minimum has direct implications for predictions of colloid transport in various natural and engineered systems. In the case of a moderate to relatively deep secondary energy well, particles are expected to exhibit a "fast" rate of deposition which approaches the transport-limited rate.[20,40] When the secondary energy minimum is more shallow, it has been hypothesized that particles are continuously deposited and released in a dynamic process.[41] Because the depth of the secondary energy well and the height of the energy barrier are directly propor-

(20) Tufenkji, N.; Elimelech, M. *Langmuir* **2004**, *20*, 10881−10828.
(21) Elimelech, M.; O'Melia, C. R. *Environ. Sci. Technol.* **1990**, *24*, 1528−1536.
(22) Hull, M.; Kitchener, J. A. *J. Chem. Soc., Faraday Trans.* **1969**, *65*, 3093.
(23) Bowen, B. D.; Epstein, M. *J. Colloid Interface Sci.* **1979**, *72*, 81.
(24) Gregory, J.; Wishart, A. J. *Colloids Surf.* **1980**, *1*, 313.
(25) Kihira, H.; Ryde, N.; Matijevic, E. *J. Chem. Soc., Faraday Trans.* **1992**, *88*, 2379−2386.
(26) Kihira, H.; Matijevic, E. *Langmuir* **1992**, *8*, 2855−2862.
(27) Derjaguin, B. V.; Landau, L. D. *Acta Physicochim. URSS* **1941**, *14*, 733−762.
(28) Verwey, E. J. W.; Overbeek, J. T. G. *Theory of the Stability of Lyophobic Colloids*; Elsevier: Amsterdam, 1948.
(29) Litton, G. M.; Olson, T. M. *J. Colloid Interface Sci.* **1994**, *165*, 522−525.
(30) Litton, G. M.; Olson, T. M. *Environ. Sci. Technol.* **1993**, *27*, 185−193.
(31) Song, L. F.; Johnson, P. R.; Elimelech, M. *Environ. Sci. Technol.* **1994**, *28*, 1164−1171.
(32) Chen, J. Y.; Ko, C. H.; Bhattacharjee, S.; Elimelech, M. *Colloid Surf., A* **2001**, *191*, 3−15.
(33) Elimelech, M.; Nagai, M.; Ko, C. H.; Ryan, J. N. *Environ. Sci. Technol.* **2000**, *34*, 2143−2148.
(34) Song, L. F.; Elimelech, M. *J. Chem. Soc., Faraday Trans.* **1993**, *89*, 3443−3452.
(35) Tobiason, J. E. Ph.D. Dissertation, The Johns Hopkins University, 1987.
(36) Elimelech, M. Ph.D. Dissertation, The Johns Hopkins University, 1989.
(37) Litton, G. M.; Olson, T. M. *Colloid Surf., A* **1996**, *107*, 273−283.
(38) Hahn, M. W.; Abadzic, D.; O'Melia, C. R. *Environ. Sci. Technol.* **2004**, *38*, 5915−5924.
(39) Redman, J. A.; Walker, S. L.; Elimelech, M. *Environ. Sci. Technol.* **2004**, *38*, 1777−1785.
(40) Hahn, M. W.; O'Melia, C. R. *Environ. Sci. Technol.* **2004**, *38*, 210−220.
(41) Franchi, A.; O'Melia, C. R. *Environ. Sci. Technol.* **2003**, *37*, 1122−1129.
(42) Ruckenstein, E.; Prieve, D. C. *J. Chem. Soc., Faraday Trans. 2* **1973**, *69*, 1522−1536.
(43) Elimelech, M.; Gregory, J.; Jia, X.; Williams, R. A. *Particle Deposition and Aggregation: Measurement, Modelling, and Simulation*; Butterworth-Heinemann: Oxford, England, 1995.
(44) Adamczyk, Z.; Czarnecki, J.; Dabros, T.; van de Ven, T. G. M. *Adv. Colloid Interface Sci.* **1983**, *19*, 183−252.
(45) Spielman, L. A.; Friedlander, S. K. *J. Colloid Interface Sci.* **1974**, *46*, 22−31.
(46) McDowell-Boyer, L. M. *Environ. Sci. Technol.* **1992**, *26*, 586−593.

tional to particle size, it is expected that secondary minimum deposition will be more important for larger particles.

The objective of this paper is to unravel the mechanisms and causes of deviation from CFT. The deposition behavior of uniform polystyrene latex particles in columns packed with spherical glass beads was examined over a wide range of physicochemical conditions, whereby both the fluid-phase effluent particle concentration and the profile of retained particles were measured. In a first set of experiments, the role of the secondary energy minimum in deviation from CFT was examined by comparing the deposition behavior of three different-sized particles in a simple background electrolyte solution. In an effort to mask near-neutrally charged regions of particle and collector surfaces, a second series of experiments was conducted with addition of anionic surfactant to background electrolyte solutions. To further verify the validity of CFT, a third set of experiments was conducted using solutions of high pH to mask the influence of metal oxide impurities on glass bead surfaces. We demonstrate that both secondary minimum deposition and surface charge heterogeneities are the main causes for the deviation from CFT generally observed in colloid deposition studies. We further show that agreement with CFT is observed even in the presence of a repulsive energy barrier, suggesting that it is not the general existence of repulsive colloidal interactions which causes deviation but more precisely the occurrence of multiple particle deposition rates.

2. Materials and Methods

2.1. Colloidal Particles and Porous Media. Three different sizes (63, 320, and 3000 nm) of surfactant-free fluorescent polystyrene latex colloids (Interfacial Dynamics Corporation, Portland, OR) with carboxyl-modified functional groups were used as model particles. The density of the particles, as reported by the manufacturer, is 1.055 g/cm^3.

Spherical soda-lime glass beads (Class V, MO-SCI Corporation, Rolla, MO) were used as model collector grains. The manufacturer reported the average diameter of the glass beads as 0.33 mm. The chemical composition (by weight) of the beads is as follows: ~70% SiO_2, ~3% Al_2O_3, ~10% CaO, ~3% MgO, ~15% Na_2O, <0.3% Fe_2O_3. The glass beads were thoroughly cleaned to remove grease and other impurities as described elsewhere.[20]

2.2. Solution Chemistry. Analytical reagent-grade KCl (Fisher Scientific) and deionized (DI) water were used to prepare electrolyte solutions. Salt concentrations were varied over a wide range of ionic strengths (3−300 mM) so that *favorable* and *unfavorable* deposition could be studied. The pH of the suspensions was adjusted to 8 by addition of $KHCO_3$ (1 mM). In a second series of experiments, 0.06 mM sodium dodecyl sulfate (SDS) (Fisher Scientific) was added to the background electrolyte solution. A third set of experiments was conducted where the pH of the suspensions was adjusted to 11 by addition of NaOH (1 mM).

2.3. Electrokinetic Characterization of Particles and Collectors. Microelectrophoresis (ZetaPALS, Brookhaven Instruments Corporation, Holtsville, NY) was used to characterize the electrokinetic properties of the latex particles over the range of solution chemistries used in the column experiments. Electrophoretic mobility was measured at 25 °C (±1 °C) using particle suspensions (7.2×10^{10}, 3.5×10^8, and 4.7×10^5 particles/mL for the 63, 320, and 3000 nm particles, respectively) prepared in the background electrolyte of interest. Electrophoretic mobilities of the smaller particles (63 and 320 nm) were converted to zeta potentials using tabulated numerical calculations of Ottewill and Shaw.[47] Zeta potentials of the 3000 nm particles were calculated from the measured electrophoretic mobilities using the Smoluchowski equation.[48] The electrokinetic properties of the glass beads were measured over the range of solution conditions used in the column experiments as described elsewhere.[20]

2.4. Column Deposition Experiments. Experiments were conducted by pumping a suspension of latex particles through a glass chromatography column packed with clean soda-lime glass beads. An adjustable-height column (C 16/20, Amersham Biosciences, Piscataway, NJ) with an inner diameter of 1.6 cm was used. The soda-lime glass beads were wet-packed to a height of 12.6 cm with vibration to minimize any layering or air entrapment. Standard gravimetric methods were used to determine the glass bead density (2.43 g/cm^3) and a column packing porosity of 0.37.

The packed column was equilibrated by pumping (model 200 syringe pump, KD Scientific Inc., New Hope, PA) 20 pore volumes of the particle-free electrolyte solution through the column at a constant approach (superficial) velocity of 8.3×10^{-3} cm/s. A suspension of latex colloids of the same electrolyte composition was pumped for 2.8 pore volumes followed by an equivalent injection of a particle-free electrolyte solution. Particle concentration at the column outlet was monitored on-line using measurements of fluorescence intensity (EX/EM 509/574 and EX/EM 360/402 for 63 and 320 nm particles, respectively) with a spectrofluorometer (FluoroMax-3, Jobin Yvon Horiba, Edison, NJ). For experiments conducted with the largest particles (3000 nm), the effluent particle concentration was measured on-line using a UV/visible spectrophotometer (at 360 nm) (Hewlett-Packard model 8453) and a 1 cm flow-through cell. For these larger sized particles, a constant influent concentration (C_0) was maintained by including a miniature magnetic stir bar in the particle solution syringe. The influent particle concentration was varied between experiments to obtain optimal resolution; specifically, we used C_0 ~10^9, ~5×10^7, and ~10^7 particles/mL for experiments conducted with 63, 320, and 3000 nm particles, respectively. Column experiments were conducted over a different range of ionic strengths for each particle size such as to obtain comparable degrees of removal. In each experiment, the total amount of retained particles (N_{dep}) was determined by calculating the difference between the number of particles injected into the column (N_{inj}) and the amount obtained by numerically integrating the particle breakthrough curve (N_{effl}). In experiments conducted with anionic surfactant, 0.06 mM SDS was added to the background electrolyte solutions in all steps of the experiment (i.e., during equilibration, injection of particles, and postinjection of particles).

2.5. Column Dissection and Measurement of Retained Particles. After completing a colloid deposition experiment, the packed bed was dissected into sections to obtain the profile of retained particles in the column. In experiments conducted with 3000 nm particles, retained particle concentrations were determined using a fluorescent microscope as we described elsewhere.[20] However, for experiments conducted with 63 and 320 nm particles, particle concentrations in each packed-bed section were determined by measuring the fluorescence intensity of representative 0.2 mL samples of supernatant solutions in a spectrofluorometer. At the conclusion of each experiment, the soda-lime glass beads were discarded.

In each experiment, the mass balance of latex particles was determined by comparing the number of deposited particles calculated from integrating the particle breakthrough curve (N_{dep}) to the amount retained based on measurement in the spectrofluorometer or enumeration in the fluorescent microscope. In general, the mass balance was found to be within ±17%, but in most experiments the mass balance was ±8%.

2.6. Determination of Attachment (Collision) Efficiency. To quantitatively compare the experiments conducted with three different sized particles under changing solution conditions, values of the particle attachment (collision) efficiency, α, were calculated.[10,49] The attachment efficiency is defined as the ratio of the experimental single-collector removal efficiency (η) and the predicted single-collector contact efficiency (η_0) evaluated from solution of the convective-diffusion equation in the absence of repulsive interaction energies, i.e., $\alpha = \eta/\eta_0$.[10,21,50] Values of

(47) Ottewill, R. H.; Shaw, J. N. *J. Electroanal. Chem.* **1972**, *37*, 133−142.

(48) Masliyah, J. H. *Electrokinetic Transport Phenomena*; AOSTRA: Edmonton, AB, 1994.

(49) Grolimund, D.; Elimelech, M.; Borkovec, M.; Barmettler, K.; Kretzschmar, R.; Sticher, H. *Environ. Sci. Technol.* **1998**, *32*, 3562−3569.

η_0 for the described experimental conditions were determined using a newly developed correlation based on a rigorous numerical solution of the convective-diffusion equation:[50]

$$\eta_0 = 2.4A_S^{1/3} N_R^{-0.081} N_{Pe}^{-0.715} N_{vdW}^{0.052} + 0.55A_S N_R^{1.675} N_A^{0.125} + 0.22N_R^{-0.24} N_G^{1.11} N_{vdW}^{0.053} \quad (1)$$

where N_R is an aspect ratio, N_{Pe} is the Peclet number, N_A is the attraction number, N_{vdW} is the van der Waals number, and N_G is the gravity number.

The experimental single-collector removal efficiency, η, was determined from each particle breakthrough curve as follows:

$$\eta = -\frac{2}{3}\frac{d_c}{(1-\epsilon)L}\ln(C/C_0) \quad (2)$$

where d_c is the diameter of the collector grains, ϵ is the bed porosity, and L is the packed bed length. The normalized column effluent concentration (C/C_0) in eq 2 was obtained from each particle breakthrough curve by averaging the values measured between pore volumes 1.8 and 2 (i.e., $1050 < t < 1166$ s).

Particle attachment efficiencies can also be calculated directly from the profile of retained particles, $S(x)$:

$$S(x) = \frac{t_0\epsilon k}{\rho_b} C(x) = \frac{t_0\epsilon k C_0}{\rho_b}\exp\left[-\frac{k}{v}x\right] \quad (3)$$

Here, k is the particle deposition rate coefficient, v the interstitial particle velocity, ρ_b the porous medium bulk density, and t_0 the duration of continuous particle injection at concentration C_0 (at $x = 0$). The particle deposition rate coefficient, k, is related to the commonly used single-collector removal efficiency η via[10,49,50]

$$k = \frac{3(1-\epsilon)v}{2d_c}\eta \quad (4)$$

Linearization of eq 3 reveals that the particle deposition rate coefficient, k, and thus the attachment efficiency, α, can be obtained from both the intercept and slope of a semilog plot of $S(x)$:

$$\ln S(x) = \ln\left(\frac{t_0\epsilon C_0}{\rho_b}k\right) - \frac{k}{v}x \quad (5)$$

where $k = \alpha k_{fav}$ and k_{fav} is related to η_0 via eq 4. For each experiment, the value of the attachment efficiency was calculated from the intercept (α_{INT}) and slope (α_{SLOPE}) of a semilog plot of the retained particle profile, $S(x)$.

3. Results and Discussion

3.1. Electrokinetic Properties of Colloids and Collectors. The zeta (ζ) potentials of the latex colloids and soda-lime glass beads over the range of solution chemistries used in the column experiments are presented in Table 1. Both the particles and the glass beads are negatively charged under the conditions investigated, and their zeta potentials become more negative with decreasing ionic strength. Addition of SDS had little influence on the measurements for the glass beads, whereas the zeta potentials of the 320 and 3000 nm particles were generally 7 mV more negative than those obtained in the absence of SDS. These observations are consistent with those of Litton and Olson[29] who studied the influence of SDS on latex colloids and quartz sand. Anionic surfactants, such as SDS, are known to mask uncharged or slightly positively charged regions of latex and silica surfaces,[22,29] resulting in a more homogeneous charge distribution on the particle and collector surfaces. In general, an increase in pH resulted in little change in the glass bead zeta potentials. However, the latex particles are slightly more negatively charged at pH 11 than at pH 8. At this higher pH, both the carboxyl latex and the glass bead surfaces are completely deprotonated. In addition, since pH 11 is near or above the isoelectric point of any metal oxides (Al_2O_3, CaO, MgO, Na_2O, and Fe_2O_3) found on the glass bead surface, these surface impurities will also carry a negative charge under this condition. Measured zeta potentials are used later to calculate DLVO interaction energy profiles for the different latex particle−glass bead systems.

Table 1. Electrokinetic Properties of Latex Particles and Glass Bead Collectors

ionic strength (mM)	pH	zeta potential (mV) 63 nm latex	320 nm latex	3000 nm latex	glass beads
3	8	*a*	*a*	−80.3	−55.2
10	8	*a*	*a*	−60.5	−50.2
20	8	−58.5	−70.6	*a*	−42.7
30	8	−55.2	−54.0	−45.3	−36.6
40	8	−50.3	−46.7	*a*	−32.5
100	8	*a*	−37.6	−30.1	−18.9
300	8	*a*	−26.4	−27.9	−15.7
20 + 0.06 mM SDS	8	*a*	−73.6	*a*	−42.7
30 + 0.06 mM SDS	8	*a*	−63.8	−56.0	−38.0
40 + 0.06 mM SDS	8	*a*	−53.8	*a*	−37.5
50 + 0.06 mM SDS	8	*a*	*a*	−44.1	−34.5
100 + 0.06 mM SDS	8	*a*	*a*	−35.3	−24.3
80	11	−39.4	−44.9	*a*	−28.8
100	11	−33.0	−41.7	−38.2	−21.9
200	11	−24.8	−32.3	−31.5	−16.3

[a] Not measured (i.e., column experiment not conducted under given condition).

3.2. Role of Particle Size in Breakdown of CFT. As described earlier, several researchers have observed microbial deposition behavior which deviates from that predicted by classical CFT.[11−16] In our previous work,[20] we demonstrated how CFT breaks down in the presence of repulsive electrostatic interactions, even for the case of model colloidal particles depositing in columns packed with uniform spherical collectors. We proposed that particle deposition in a secondary energy minimum could contribute to the observed deviation from CFT.[20] Within the context of the DLVO theory of colloidal stability,[27,28] the height of the energy barrier (Φ_{max}) and the depth of the secondary energy well ($\Phi_{2°min}$) are directly proportional to particle size. In this section, we present well-controlled column deposition experiments conducted with three different-sized latex particles to elucidate the role of secondary minimum deposition on the deviation from CFT.

3.2.1. Particle Breakthrough Curves for Different-Sized Particles. Representative particle breakthrough curves obtained at pH 8 over a range of solution ionic strengths with 63, 320, and 3000 nm particles are presented in Figure 1. In these breakthrough curves, the normalized effluent particle concentration (C/C_0) is plotted as a function of time. As expected, the deposition of latex colloids on the glass beads increases (C/C_0 decreases) with increasing ionic strength. As the concentration of KCl in the solution increases, the diffuse double layers are compressed causing a reduction in the repulsive electrostatic double-layer forces and an increase in the particle deposition (removal) rate.

To quantitatively compare the colloid transport experiments, the particle attachment efficiency, α_{BTC}, was determined from each particle breakthrough curve. The attachment efficiency depends on the colloidal interactions between particles and collectors; it approaches unity when colloidal interactions are *favorable* for deposition and is

(50) Tufenkji, N.; Elimelech, M. *Environ. Sci. Technol.* **2004**, *38*, 529−536.

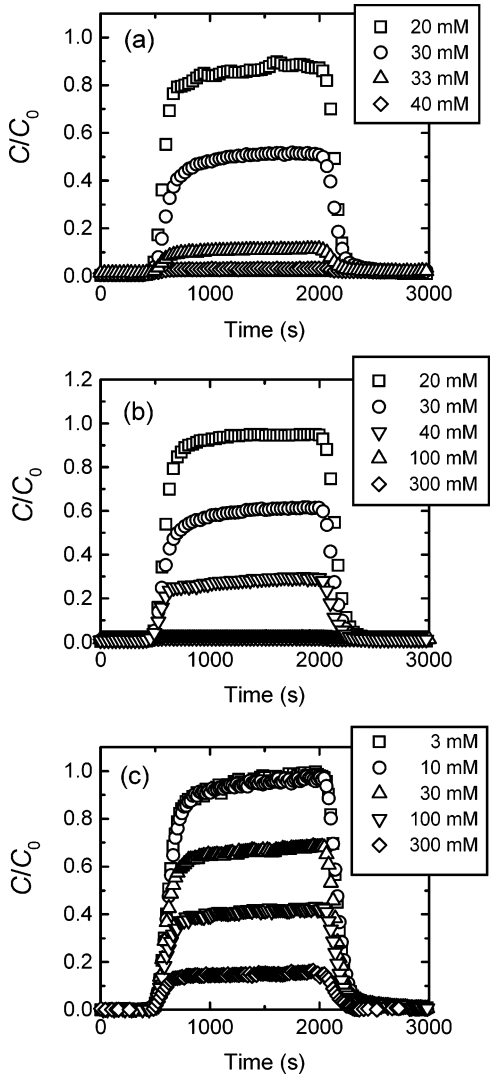

Figure 1. Representative breakthrough curves for experiments conducted with (a) 63, (b) 320, and (c) 3000 nm latex particles in columns packed with soda-lime glass beads over a wide range of solution ionic strengths. Key experimental conditions were as follows: approach velocity = 8.3×10^{-3} cm/s, porosity = 0.37, mean bead diameter = 0.33 mm, pH = 8.0−8.3, and temperature = 20−22 °C.

much smaller than 1 under *unfavorable* conditions (i.e., when repulsive interactions predominate). Particle attachment efficiencies (α_{BTC}) were taken as the ratio of the experimental single-collector removal efficiency (η, calculated from the normalized effluent particle concentration C/C_0 and eq 2) to the single-collector contact efficiency (η_0, given by eq 1). Values of α_{BTC} for experiments conducted at pH 8 are presented in Table 2 as a function of solution ionic strength and particle size (with other parameters to be discussed later). The observed deposition behavior follows the trend predicted by DLVO theory. For example, an increase in salt concentration from 20 to 40 mM yields an increase in α_{BTC} from 0.0096 to 0.20 for the 63 nm latex particle. Similarly, an increase in ionic strength from 20 to 300 mM results in a change in α_{BTC} from 0.0058 to 0.83 for the 320 nm particle. This large variation in values of the attachment efficiency corresponds to a shift in conditions considered *unfavorable* for deposition at the lower ionic strengths to completely *favorable* deposition at the highest ionic strengths investigated.

3.2.2. Spatial Distributions of Retained Particles. Following the completion of each particle deposition experiment, the spatial distribution of retained particles was determined by carefully dissecting the packed bed. In Figure 2, representative profiles of retained particles corresponding to the breakthrough curves in Figure 1 are presented. The normalized retained particle concentration, $S(x)/C_0$, is plotted as a function of distance in a semilog format. For comparison, the profile of retained particles predicted by CFT (eq 3) using the attachment efficiency determined from the corresponding particle breakthrough curve (α_{BTC}) is included in each figure (solid lines).

If the classical CFT were valid under these physicochemical conditions, the spatial distribution of particles determined experimentally should be virtually identical to the spatial distribution calculated using eq 3 and values of α_{BTC}. However, inspection of Figure 2 reveals that the measured concentrations are in marked discrepancy with those predicted by CFT, with the exception of those measured at the higher ionic strengths. This observed behavior is consistent with previously reported findings using model colloids and bacteria.[15,20]

3.2.3. Attachment Efficiencies for Different-Sized Particles. To study the effect of particle size and solution ionic strength on the deviation from CFT, the value of the attachment efficiency, α_{SLOPE}, was calculated from the slope of each profile of retained particles, $S(x)$, and compared with values of α calculated from the corresponding particle breakthrough curve, α_{BTC} (Figure 3). In such a plot, data points falling on the dashed line (slope of 1 and intercept of zero) indicate perfect agreement between values of the attachment efficiency calculated from the slope of the retained profile (α_{SLOPE}) and the attachment efficiency determined from the particle breakthrough curve (α_{BTC}). As mentioned previously in Materials and Methods, values of the attachment efficiency were also calculated from the intercept (α_{INT}) of a semilog plot of $S(x)$. Comparison of calculated values of α_{INT} with α_{BTC} show the same general trend as values of α_{SLOPE}. However, α_{INT} does not vary over such a wide range as α_{SLOPE}, and as a result, the trend in the data is not as clear. Hence, for the sake of clarity, we focus on the comparison of α_{BTC} and α_{SLOPE}.

The comparison shown in Figure 3 emphasizes the paramount role of particle size and solution ionic strength on the deviation from CFT. At the higher ionic strengths investigated (40, 100, and 300 mM for the 63, 320, and 3000 nm particles, respectively), calculated values of α_{BTC} are nearly identical to corresponding values of α_{SLOPE} (i.e., data points fall on the dashed line). As the solution salt concentration decreases (i.e., decreasing values of α_{BTC} on the y-axis), the deviation between values of α_{BTC} and α_{SLOPE} increases notably for all three particle sizes. We have recently proposed that this increased digression with decreasing ionic strength can be attributed to the concurrent existence of both *favorable* and *unfavorable* colloidal interactions in the presence of repulsive electrostatic double-layer (EDL) interactions.[20] A potential source of "fast" or *favorable* deposition sites is the presence of a secondary energy minimum in the particle-collector DLVO interaction energy profile.[20] Hence, to better understand the role of the secondary energy minimum in the observed deviation from classical CFT, DLVO theory is used to calculate colloidal interaction energies.

3.2.4. DLVO Interpretation of Particle Size Effect: Role of the Secondary Minimum. In Figure 4, DLVO interaction energy profiles for the three latex particle−glass bead systems are presented at the different solution conditions used in the deposition experiments. The total interaction energy, namely, the sum of attractive van der Waals (VDW) and repulsive EDL interactions,

Table 2. Summary of Deposition Experiments with Different Latex Particles and Calculated DLVO Interaction Parameters

run	ionic strength (mM)	pH	particle size (nm)	C_0 (particles/mL)	C/C_0[a]	α_{BTC}[b]	Φ_{max} (k_BT)	$\Phi_{2°min}$ (k_BT)
1	20	8	63	3.6×10^9	0.84	0.0096	72	0.17
2	30	8	63	2.2×10^9	0.48	0.042	50	0.28
3	33	8	63	5.8×10^8	0.10	0.13	46	0.31
4	40	8	63	8.7×10^8	0.029	0.20	35	0.40
5	20	8	320	6.6×10^7	0.97	0.0058	430	0.82
6	20	8	320	6.6×10^7	0.93	0.014	430	0.82
7	30	8	320	2.8×10^7	0.54	0.13	250	1.4
8	30	8	320	2.8×10^7	0.57	0.11	250	1.4
9	40	8	320	5.5×10^7	0.26	0.28	160	2.1
10	40	8	320	1.7×10^7	0.26	0.27	160	2.1
11	100	8	320	1.7×10^7	0.016	0.83	12	6.9
12	100	8	320	1.7×10^7	0.018	0.82	12	6.9
13	300	8	320	1.7×10^7	0.016	0.83	*c*	*c*
14	300	8	320	1.7×10^7	0.019	0.80	*c*	*c*
15	3	8	3000	1.8×10^7	0.95	0.019	7500	0.85
16	3	8	3000	2.0×10^7	0.91	0.032	7500	0.85
17	3	8	3000	1.8×10^7	0.93	0.026	7500	0.85
18	10	8	3000	1.0×10^7	0.89	0.039	4800	3.6
19	10	8	3000	1.0×10^7	0.91	0.032	4800	3.6
20	30	8	3000	1.0×10^7	0.64	0.15	1900	14
21	30	8	3000	1.0×10^7	0.68	0.13	1900	14
22	100	8	3000	4.7×10^6	0.41	0.31	12	72
23	100	8	3000	5.0×10^6	0.38	0.33	12	72
24	300	8	3000	5.1×10^6	0.14	0.67	*c*	*c*
25	300	8	3000	5.1×10^6	0.14	0.68	*c*	*c*
26	20 + 0.06 mM SDS	8	320	6.6×10^7	0.97	0.0066	440	0.81
27	30 + 0.06 mM SDS	8	320	2.8×10^7	0.75	0.058	310	1.3
28	40 + 0.06 mM SDS	8	320	2.8×10^7	0.37	0.20	243	1.9
29	30 + 0.06 mM SDS	8	3000	1.5×10^7	0.91	0.031	2600	13
30	30 + 0.06 mM SDS	8	3000	1.5×10^7	0.92	0.027	2600	13
31	50 + 0.06 mM SDS	8	3000	5.2×10^6	0.66	0.15	1500	24
32	50 + 0.06 mM SDS	8	3000	5.1×10^6	0.64	0.16	1500	24
33	100 + 0.06 mM SDS	8	3000	5.4×10^6	0.25	0.47	290	60
34	80	11	63	3.6×10^9	0.63	0.026	15	0.90
35	100	11	63	1.4×10^9	0.56	0.033	3.1	1.4
36	100	11	63	1.4×10^9	0.58	0.031	3.1	1.4
37	200	11	63	3.6×10^8	0.041	0.18	*c*	*c*
38	80	11	320	5.5×10^7	0.78	0.050	94	4.4
39	80	11	320	2.8×10^7	0.76	0.054	94	4.4
40	100	11	320	2.8×10^7	0.68	0.079	33	6.2
41	200	11	320	1.7×10^7	0.17	0.36	*c*	*c*
42	100	11	3000	1.4×10^7	0.92	0.029	246	60
43	200	11	3000	4.7×10^6	0.64	0.15	*c*	*c*

[a] Determined by averaging over pore volumes 1.8−2, as described in the text. [b] Calculated from eq 2 and $\alpha = \eta/\eta_0$. Values of the single-collector contact efficiency ($\eta_0 = 4.8 \times 10^{-2}$, 1.4×10^{-2}, and 7.9×10^{-3} for 63, 320, and 3000 nm particles, respectively) were calculated using eq 1 and the following parameter values: $d_c = 330$ μm, $U = 8.3 \times 10^{-5}$ m/s, $A = 1 \times 10^{-20}$ J, $T = 293$ K, $\rho_p = 1055$ kg/m^3, $\rho_f = 1000$ kg/m^3, $\mu = 1.005 \times 10^{-3}$ kg/m s, $\epsilon = 0.37$. [c] No energy barrier to deposition predicted.

was determined by treating the particle−glass bead system as a sphere−plate interaction. Constant-potential EDL interactions were calculated using the expression of Hogg et al.,[51] where the zeta potentials of the latex colloids and the soda-lime glass beads (Table 1) were used in place of the respective surface potentials. The retarded VDW attractive interaction energy was calculated from the expression proposed by Gregory.[52] A value of 1×10^{-20} J was chosen for the Hamaker constant of the glass−water−polystyrene system.[2,21,53]

The DLVO calculations reveal the presence of a sizable repulsive energy barrier to deposition at nearly all ionic strengths for all three particle sizes. In contrast, no energy barrier to deposition (i.e., completely *favorable* conditions) is predicted at 300 mM for the 320 and 3000 nm particles. Hence, based on DLVO interaction energy calculations, latex particles are not expected to deposit onto the glass bead surfaces (i.e., overcome the repulsive energy barrier) under these solution conditions (except at 300 mM). Despite these DLVO predictions, however, particle deposition is observed even at the lower ionic strengths examined.

In Figure 5, where the DLVO interaction energy profiles are replotted on a different scale, we note the presence of a secondary energy well at a greater separation distance than that of the energy barrier. The height of the energy barrier (Φ_{max}) and the depth of the secondary minimum ($\Phi_{2°min}$) for the three latex particle−glass bead systems are listed in Table 2 as a function of solution ionic strength and particle size. DLVO calculations indicate that the magnitude of $\Phi_{2°min}$ increases with salt concentration and particle size: ranging from 0.17 k_BT at 20 mM for the 63 nm colloid to 72 k_BT at 100 mM for the 3000 nm colloid.

Because the depth of the secondary energy minimum is directly proportional to particle size, whereby a larger particle will experience a deeper energy well, a decrease in particle size should eliminate the contribution of this *favorable* deposition site. Careful inspection of Figure 3 reveals that the deviation from CFT (i.e., the difference

(51) Hogg, R.; Healy, T. W.; Fuerstenau, D. W. *Trans. Faraday Soc.* **1966**, *62*, 1638−1651.
(52) Gregory, J. *J. Colloid Interface Sci.* **1981**, *83*, 138−145.
(53) Elimelech, M.; O'Melia, C. R. *Langmuir* **1990**, *6*, 1153−1163.

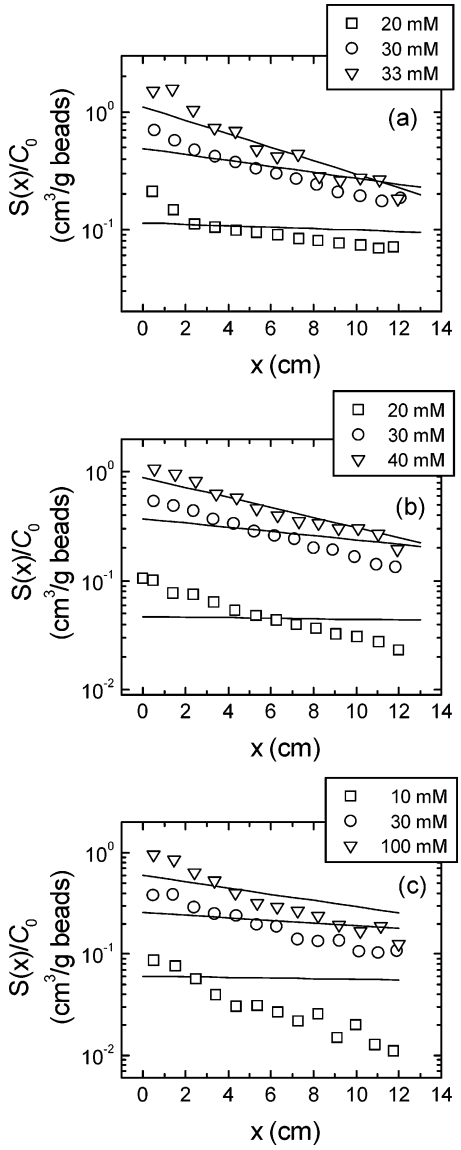

Figure 2. Comparison of representative experimental retained particle concentration profiles (symbols) and predictions based on classical CFT using α_{BTC} determined from the corresponding breakthrough curve (solid lines) for experiments conducted with (a) 63, (b) 320, and (c) 3000 nm latex particles over a range of solution ionic strengths. Experimental conditions were the same as those given in Figure 1 and are summarized in Table 2.

between values of α_{SLOPE} and corresponding α_{BTC}) decreases with decreasing particle size. In the plot of α_{BTC} versus α_{SLOPE}, the results obtained with the largest colloid (3000 nm) are all at the extreme right of the graph, and therefore furthest from the dashed line of equivalence. The data obtained with the 320 nm latex particle are considerably closer to the dashed line in the figure. However, the results obtained with the smallest (63 nm) particles show the least degree of deviation from CFT (i.e., data points are closest to the dashed line in Figure 3). This notable improvement in predictions based on classical CFT can be directly linked to a reduction in $\Phi_{2^\circ min}$ with decreasing particle size (Table 2). For instance, at 100 mM the calculated depth of the secondary energy minimum for the 3000 nm colloid is 72 k_BT, whereas the 320 nm particle experiences an attractive energy of only 6.9 k_BT. The results of these experiments indicate that "fast" deposition into the secondary energy minimum can cause significant deviation from CFT.

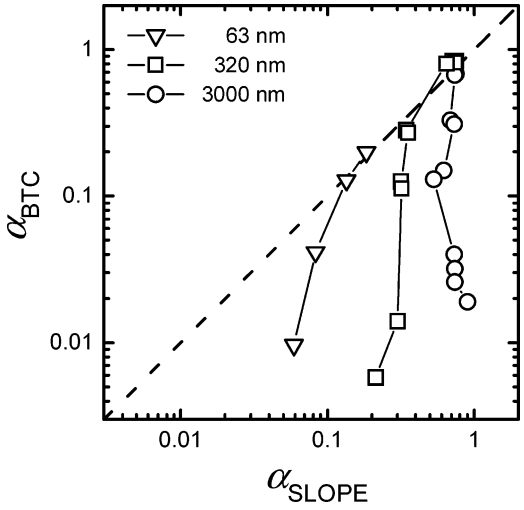

Figure 3. Comparison of attachment efficiencies determined from slope of retained particle profiles (α_{SLOPE}) and attachment efficiencies calculated from particle breakthrough curves (α_{BTC}) for (▽) 63, (□) 320, and (○) 3000 nm latex particles. Experimental conditions were the same as those given in Figure 1 and are summarized in Table 2.

3.3. Role of Surface Charge Heterogeneities: Colloid Deposition in the Presence of SDS. In the previous section, we showed how predictions of particle transport based on CFT can be improved considerably by eliminating the presence of the secondary energy well. However, inspection of Figure 3 reveals that even for the smallest colloid (63 nm), values of α_{BTC} are not in good agreement with corresponding values of α_{SLOPE} at the lower ionic strengths investigated. This suggests that an additional source of deviation may be contributing to the observed particle deposition behavior.

It has been demonstrated that surface charge heterogeneities on particle and/or collector surfaces can control particle deposition behavior under conditions deemed *unfavorable* for deposition.[29−31] Litton and Olson[29] conducted column deposition experiments in the presence of SDS using carboxyl latex colloids and ultrapure quartz sand. Their results demonstrated the strong influence of surface charge inhomogeneity on particle deposition kinetics and the effectiveness of SDS in masking near-neutrally charged regions of particle and collector surfaces. In this section, we present well-controlled column deposition experiments conducted with two different-sized latex particles in the presence of 0.06 mM SDS to clarify the role of these surface charge heterogeneities on the deviation from CFT.

3.3.1. Particle Breakthrough Curves Obtained with Addition of SDS. Transport experiments were conducted as those described in the previous section, with the exception that 0.06 mM SDS was added to the background electrolyte solutions. Representative particle breakthrough curves obtained at different solution ionic strengths (pH 8) with 320 and 3000 nm particles are presented in parts a and b of Figure 6, respectively. As described earlier, the influence of ionic strength is in qualitative agreement with DLVO theory. That is, the deposition of latex particles on the glass beads increases (C/C_0 decreases) with increasing ionic strength. Particle attachment efficiencies (α_{BTC}) were again calculated from the normalized effluent particle concentration (C/C_0) measured in each experiment using eq 2 and the value of η_0 determined from eq 1 (Table 2).

It is interesting to compare particle breakthrough curves obtained in the presence of 0.06 mM SDS with break-

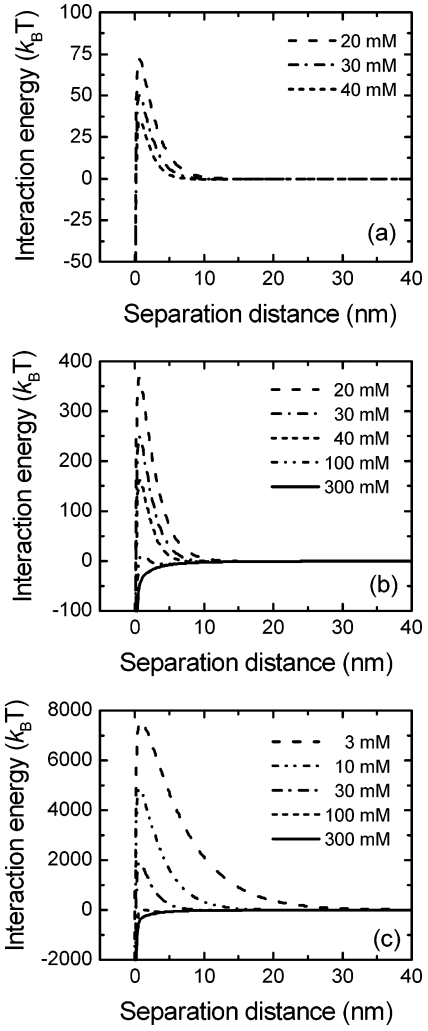

Figure 4. Calculated DLVO interaction energy plotted as a function of separation distance at different solution ionic strengths for (a) 63, (b) 320, and (c) 3000 nm latex particles. Measured zeta potentials (Table 1) and a Hamaker constant of 1×10^{-20} J were used to calculate interaction energies. Note the different scales of the *x*- and *y*-axes between the various graphs.

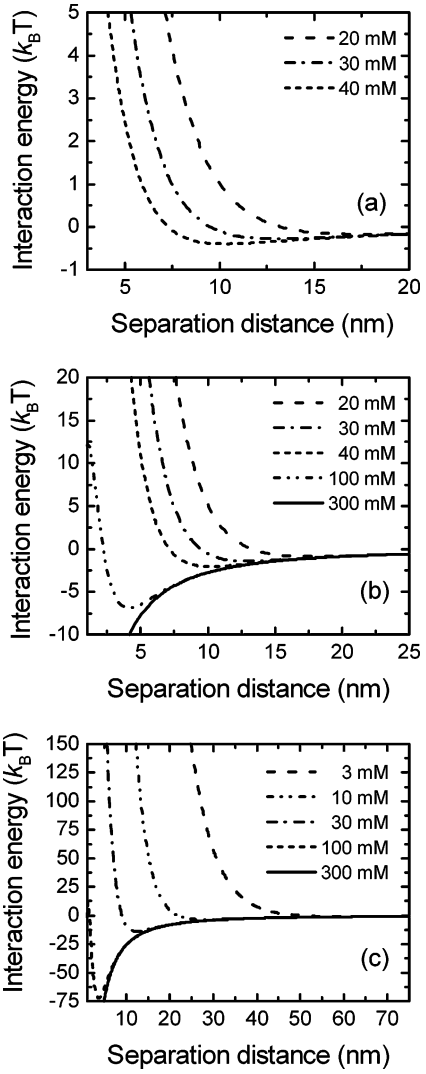

Figure 5. Data from Figure 4 are replotted to highlight the depth and location of the secondary energy minimum for (a) 63, (b) 320, and (c) 3000 nm latex particles. Note the change in scale of the *x*- and *y*-axes between the various graphs.

through curves measured without the addition of SDS (Figure 1). Comparison of the breakthrough curve obtained with the 3000 nm particle at 10 mM without SDS (Figure 1c) with that measured in the presence of SDS at a comparable degree of removal (Figure 6b, 30 mM) provides insight into the role of SDS on particle deposition behavior. In the presence of SDS, the steady state portion of the particle breakthrough curve is considerably more flat. Since the influent particle concentration (C_0) in both experiments is comparable (Table 2, runs 18 and 28), flattening of the breakthrough curve upon addition of SDS can be attributed to elimination of particle blocking on *favorable* deposition sites (i.e., surface charge heterogeneities on collector surfaces). Blocking occurs when previously deposited particles hinder subsequent deposition and is characterized by a continual increase in the effluent suspended particle concentration. As *favorable* deposition sites become blocked, the deposition rate decreases rapidly with time at surface coverages which are relatively low.[6] Because SDS masks certain surface inhomogeneities and thus eliminates the existence of these *favorable* deposition sites, particle breakthrough curves measured in the presence of SDS are noticeably flatter.

3.3.2. Spatial Distributions of Retained Particles. As described previously, the spatial distribution of retained particles was measured following each transport experiment. In Figure 7, representative profiles of retained particles corresponding to the breakthrough curves in Figure 6 are presented (closed symbols). To demonstrate the influence of SDS on the shape of the retained profile, spatial distributions measured in the absence of SDS at comparable values of initial C/C_0 (i.e., similar values of α_{BTC}) are included in each figure (open symbols). In addition, the profile of retained particles predicted by CFT (using the average value of α_{BTC} determined from the corresponding particle breakthrough curves) is included in each figure (dashed lines).

Inspection of Figure 7 reveals that the measured concentrations of retained particles deviate from those predicted by CFT (based on the average value of α_{BTC}). However, results obtained in the presence of 0.06 mM SDS are closer to model predictions. It is also interesting to note how the shape of the retained particle profiles changes upon addition of SDS. In the presence of SDS, the slope of the retained profile is clearly less steep. Because the steep slope at the top of the retained particle profile is attributed to "fast" deposition of a fraction of the particle population,[18,20] these results suggest that the

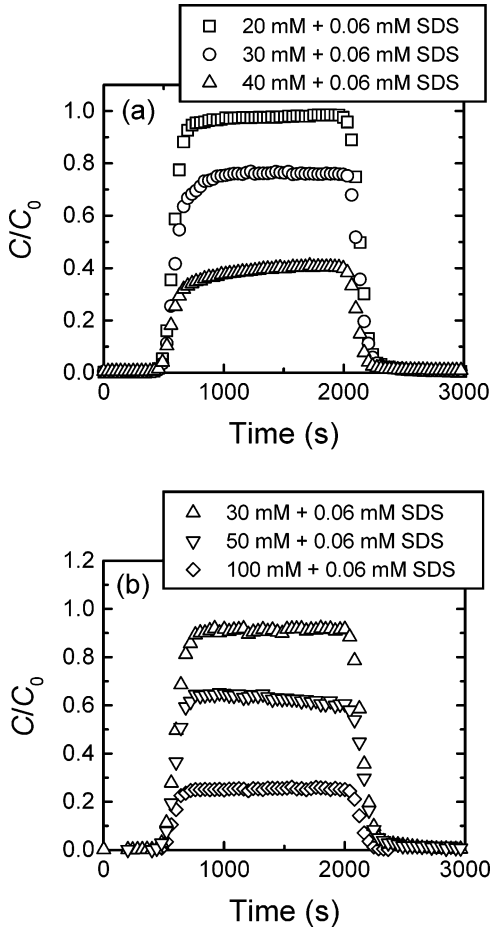

Figure 6. Representative breakthrough curves for experiments conducted in the presence of 0.06 mM SDS with (a) 320 and (b) 3000 nm latex particles in columns packed with soda-lime glass beads over a range of solution ionic strengths. Other experimental conditions were the same as those given in Figure 1 and are summarized in Table 2.

addition of SDS reduces the extent of "fast" deposition. As noted earlier, anionic surfactants such as SDS are known to mask near-neutrally charged regions of particle or collector surfaces which are considered *favorable* for deposition.[22,29] Under the solution conditions of the experiments presented here (i.e., pH 8), the dominant SDS adsorption mechanism is hydrophobic interaction between the alkyl chain of the surfactant molecule and local hydrophobic sites on particle and collector surfaces, resulting in extension of the negatively charged polar head. SDS adsorption onto metal-oxide impurities on the surface of the glass beads can also result from electrostatic interaction between the polar headgroup and these near-neutrally charged surface heterogeneities. With sufficient surfactant adsorption, the charge distribution on particle and collector surfaces becomes more homogeneous and is generally more negative. Comparison of particle breakthrough curves and retained particle profiles obtained in the absence and presence of SDS indicates that the addition of a small amount of anionic surfactant (0.06 mM) was sufficient to reduce the influence of surface charge inhomogeneities on particle and collector surfaces. The ability of SDS to mask surface charge heterogeneities and its effect on particle deposition is observed here in both flattening of particle breakthrough curves and a change in the shape of retained particle profiles. The concentration of SDS used in these experiments is relatively low, however, and we still observe deviation

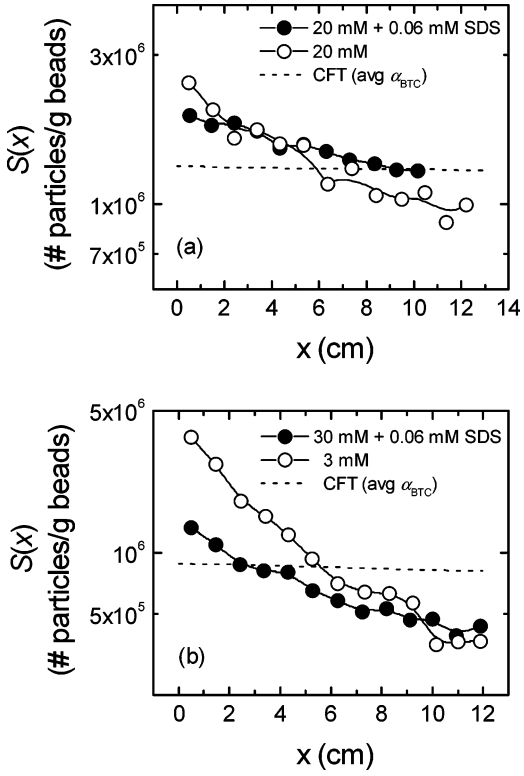

Figure 7. Comparison of retained particle concentration profiles obtained in the presence of 0.06 mM SDS (●) and without the addition of SDS (○) for experiments conducted with (a) 320 nm (runs 5 and 26, Table 2) and (b) 3000 nm latex particles (runs 16 and 29, Table 2). Predictions based on classical CFT using the average value of α_{BTC} determined from the corresponding breakthrough curves are also shown (dashed lines). Other experimental conditions were the same as those given in Figure 1 and are summarized in Table 2.

between measured and predicted profiles of retained particles.

3.3.3. Influence of SDS on Attachment Efficiencies. To quantify the influence of SDS addition on the deviation from CFT, values of α_{SLOPE} are compared to corresponding values of α_{BTC} for experiments conducted in the presence of 0.06 mM SDS (Figure 8, closed symbols). Inspection of Figure 8 reveals that the results obtained with two different sized particles with addition of SDS all fall to the left of the data obtained without surfactant (open symbols). In such a plot, this indicates that the presence of SDS in the background electrolyte solution results in improved agreement with predictions of particle transport based on CFT; that is, the closed symbols are closer to the dashed line of equivalence than the open symbols. Upon addition of SDS, surface charge heterogeneities of both the latex and silica surfaces are concealed, and thus the contribution of these sites to *favorable* particle deposition is reduced or eliminated. It is important to note that although SDS masks charge heterogeneities, it should not influence secondary minimum deposition. The observed improved agreement with CFT in the presence of SDS suggests that the secondary energy well is not the sole source of deviation. Comparison of attachment efficiencies measured with and without surfactant indicates that surface charge heterogeneities can also contribute to deviation from classical CFT.

3.4. Role of Metal Oxide Impurities: Masking Heterogeneity with High pH Solution. Inspection of Figure 8 reveals that even with addition of SDS to mask near-neutrally charged regions of particle and collector surfaces, values of α_{BTC} are not in perfect agreement with

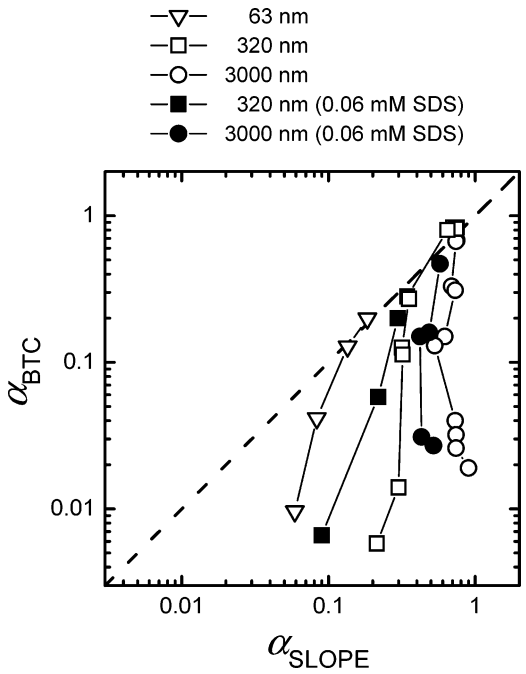

Figure 8. Comparison of attachment efficiencies determined from slope of retained particle profiles (α_{SLOPE}) and attachment efficiencies calculated from particle breakthrough curves (α_{BTC}) for (■) 320 and (●) 3000 nm latex particles in the presence of SDS. In this figure, results obtained in the presence of SDS (closed symbols) are compared to those measured without SDS addition (open symbols), previously shown in Figure 3. Other experimental conditions were the same as those given in Figure 1 and are summarized in Table 2.

corresponding values of α_{SLOPE} at the lower ionic strengths investigated. This result suggests that either (i) surface charge heterogeneities were not completely eliminated in the presence of SDS or (ii) there exists another source of deviation from CFT which was not considered. A common source of surface charge inhomogeneity that has been recognized in the literature is the presence of various metal oxide impurities (Al_2O_3, CaO, MgO, Na_2O, and Fe_2O_3) on the surface of glass bead collectors.[29−31] At the solution pH maintained in the column transport experiments (~8), the metal oxides will be near-neutrally charged or carry a slightly positive charge in comparison to the bulk SiO_2 surface which will be highly negatively charged. Hence, these surface charge heterogeneities are expected to provide *favorable* or "fast" deposition sites on what is otherwise an *unfavorable* surface for deposition.[31] In an effort to completely mask or eliminate the influence of these metal oxide impurities, additional column deposition experiments were conducted with all three latex particles in the presence of 1 mM NaOH (pH ~11). Since this higher pH is near or above the isoelectric point of the metal oxides found on the glass bead surface, these surface impurities will carry a negative charge under this condition.

3.4.1. Particle Breakthrough Curves Obtained at High pH. Representative particle breakthrough curves obtained at different solution ionic strengths (pH 11) with 63, 320, and 3000 nm particles are presented in Figure 9. In these experiments, it was found that higher salt concentrations were necessary to obtain degrees of particle removal comparable to those observed at pH 8. As before, the deposition of latex particles on the glass beads increases (C/C_0 decreases) with increasing ionic strength. Particle attachment efficiencies (α_{BTC}) were again calculated from the normalized effluent particle concentration (C/C_0) measured in each experiment using eq 2 and the value of η_0 determined from eq 1 (Table 2).

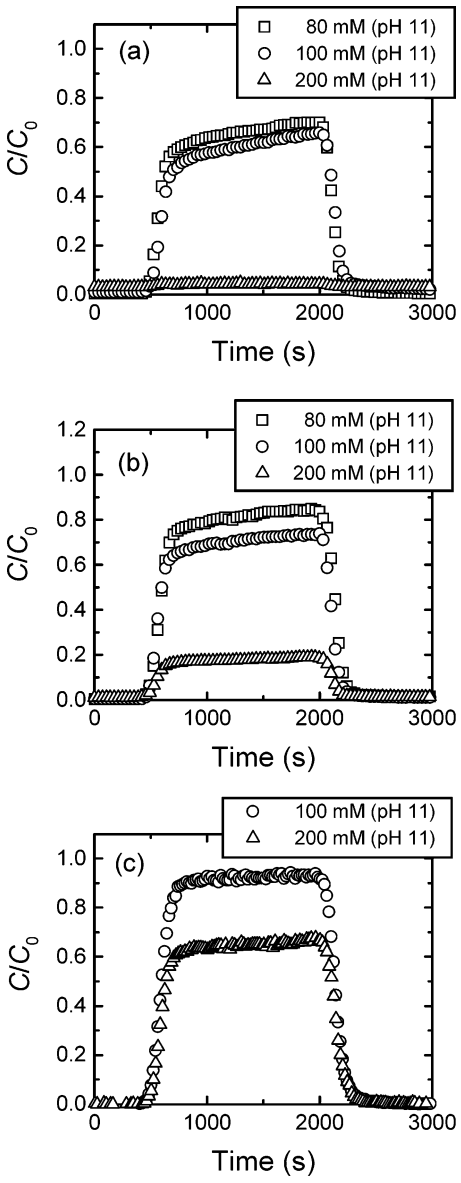

Figure 9. Representative breakthrough curves for experiments conducted at pH 11 with (a) 63, (b) 320, and (c) 3000 nm latex particles in columns packed with soda-lime glass beads over a range of solution ionic strengths. Other experimental conditions were the same as those given in Figure 1 and are summarized in Table 2.

3.4.2. Spatial Distributions of Retained Particles. In Figure 10, profiles of retained particles corresponding to the breakthrough curves in Figure 9 are presented (symbols). The normalized retained particle concentration, $S(x)/C_0$, is plotted as a function of distance in a semilog format. For comparison, the profile of retained particles predicted by CFT (eq 3) using the attachment efficiency determined from the corresponding particle breakthrough curve (α_{BTC}) is included in each figure (solid lines).

Spatial distributions of retained particles measured at pH 11 with the 63 nm latex colloid are in good agreement with predictions based on CFT over the range of ionic strengths investigated (Figure 10a). In experiments conducted with the 320 and 3000 nm particles, the measured profiles are again in accord with CFT, except at the lowest ionic strengths considered (80 and 100 mM, respectively). This marked improved agreement with CFT observed with the three different-sized colloids at relatively low degrees of particle removal (i.e., $\alpha \ll 1$) has important implications for application of CFT. In previous experiments conducted

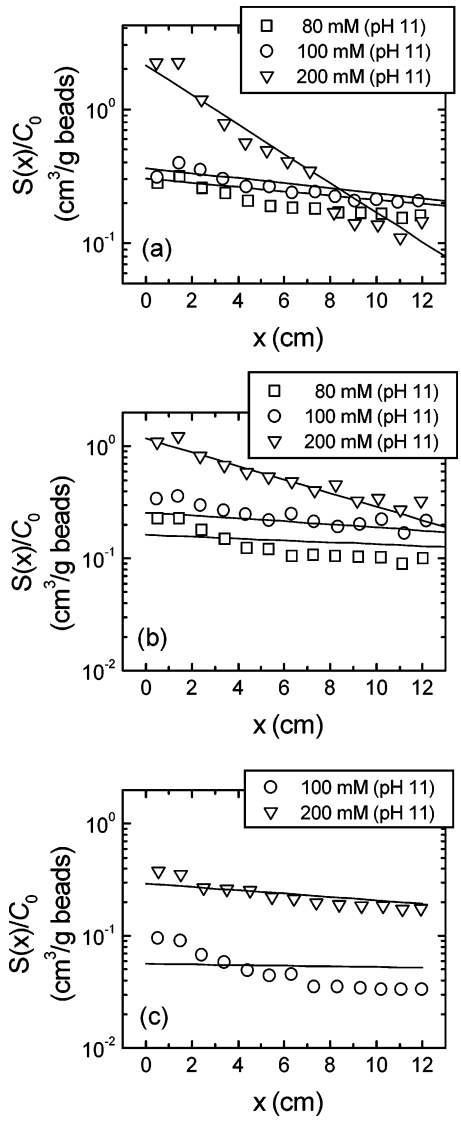

Figure 10. Comparison of experimental retained particle concentration profiles (symbols) and predictions based on classical CFT using α_{BTC} determined from the corresponding breakthrough curve (solid lines) for experiments conducted at pH 11 with (a) 63, (b) 320, and (c) 3000 nm latex particles over a range of solution ionic strengths. Other experimental conditions were the same as those given in Figure 1 and are summarized in Table 2.

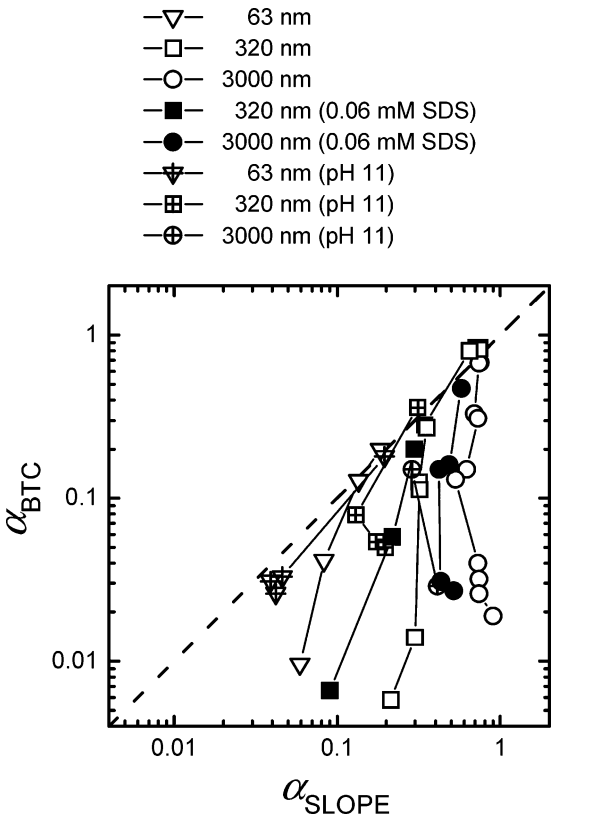

Figure 11. Comparison of attachment efficiencies determined from slope of retained particle profiles (α_{SLOPE}) and attachment efficiencies calculated from particle breakthrough curves (α_{BTC}) for experiments conducted at pH 11 with 63, 320, and 3000 nm latex particles. In this figure, results obtained at pH 11 are represented by crossed open symbols. These data are compared to all results shown previously in Figures 3 and 8, where closed symbols represent results obtained in the presence of SDS and open symbols represent those measured without SDS addition. Other experimental conditions were the same as those given in Figure 1 and are summarized in Table 2.

with model colloids in columns packed with spherical glass bead collectors, agreement with CFT was observed only under conditions deemed completely *favorable* for deposition (i.e., $\alpha \approx 1$).[20] However, calculations of DLVO interaction energy profiles for the conditions of the experiments presented here reveal the presence of an energy barrier to deposition (except at 200 mM), even for the smallest colloid (Table 2). For instance, at pH 11 the calculated height of the energy barrier for the 63 nm colloid at 80 mM is 15 k_BT and for the 320 nm colloid at 100 mM is 33 k_BT. Thus, the results of column experiments conducted at pH 11 suggest that agreement with CFT can be obtained even under conditions where repulsive electrostatic interactions dominate. When the influence of deposition mechanisms not considered in the classical theory is reduced or even completely eliminated (e.g., the contribution of surface charge heterogeneities is eliminated), the degree of deviation from CFT is considerably diminished.

3.4.3. Influence of High pH Solution on Attachment Efficiencies. The results of all deposition experiments conducted with three different-sized latex colloids under different solution conditions are summarized in Figure 11. Values of α_{SLOPE} determined from the measured profiles of retained particles are compared to corresponding values of α_{BTC}, where experiments conducted at pH 8 without SDS, at pH 8 with SDS, and at pH 11 are represented by open symbols, closed symbols, and crossed symbols, respectively.

The comparison shown in Figure 11 highlights the influence of the secondary energy minimum and surface charge heterogeneities on the deviation from CFT. For the experiments conducted with the smallest particle (63 nm) at pH 11, where the contribution of secondary minimum deposition is negligible and "fast" deposition on surface charge heterogeneities is eliminated, values of α_{SLOPE} are in good agreement with α_{BTC} over the range of ionic strengths investigated (i.e., data points fall on or near the dashed line of equivalence). As discussed in the previous section, the measured profiles of retained particles are in agreement with predictions based on CFT, even in the presence of substantial repulsive DLVO interactions. This result suggests that it is not the occurrence of an energy barrier that causes deviation from CFT. Rather, it supports our proposed mechanism that the combined influence of both "fast" and "slow" particle deposition is the key cause of the observed deviation from CFT.[20] That is, when the contributions of the secondary energy well and surface charge heterogeneities are eliminated, the sole mechanism of deposition is that of

particles overcoming the repulsive energy barrier to deposit in the primary energy well. In this particular case, measured profiles of retained particles are in good agreement with predictions based on CFT (Figures 10a and 11).

Under conditions where more than one deposition mode contributes to the overall removal of particles, the observed deposition behavior does not coincide with model predictions. For instance, when surface charge heterogeneities are masked using an anionic surfactant or a solution of high pH, the results observed for the larger particles are not as close to the dashed line of equivalence as the data for the 63 nm latex particle (Figure 11). This behavior can be attributed to the combined influence of secondary minimum deposition ("fast") and primary minimum deposition over a repulsive energy barrier ("slow"). As particle size increases, the depth and thus influence of the secondary energy minimum also increase and cannot be neglected. Furthermore, it has been shown that the degree of surface charge heterogeneity on particle and/or collector surfaces can control particle deposition behavior under conditions where repulsive DLVO interactions dominate.[29−31] Thus, the results of this work underscore the importance of considering a dual deposition mode model where the contributions of both "fast" and "slow" deposition are considered when predicting particle transport in saturated porous media.

Although the purpose of SDS addition (section 3.3) and the use of solutions of high pH were the same—to eliminate the influence of charge heterogeneities on particle and collector surfaces—we note an improved agreement with CFT in the third series of experiments in comparison to that observed in the SDS experiments (Figure 11). This may be attributed to the relatively low SDS concentration (0.06 mM) used in our experiments (e.g., compared to Litton and Olson,[29] where they used an SDS concentration of 1 mM). Such a low surfactant concentration was necessary due to experimental difficulties in measuring retained particle concentrations when higher concentrations of SDS were used.

4. Conclusion

Particle deposition or retention in the secondary energy minimum is shown to play an important role in the observed deviation from CFT. Unhindered deposition into a relatively deep secondary energy well is generally considered "fast" in comparison to deposition of particles which overcome an energy barrier to reach the primary energy minimum ("slow" deposition). Thus, the occurrence of secondary minimum deposition gives rise to a distribution in the particle deposition rate.

Addition of anionic surfactant (SDS) is shown to reduce the influence of certain surface charge heterogeneities on the deviation from CFT. The effectiveness of SDS in masking surface charge heterogeneities is also observed in flattening of particle breakthrough curves and a decrease in the slope of retained particle profiles. Furthermore, when the contribution of trace metal oxide impurities found on the surface of glass bead collectors is completely eliminated, agreement with CFT is significantly improved. Thus, surface charge heterogeneities on particle and/or collector surfaces also play an important role in the observed breakdown of CFT. Under conditions where a single deposition mechanism dominates (i.e., secondary energy well and surface charge heterogeneities are eliminated), measured profiles of retained particles are in very good agreement with predictions based on classical CFT.

It is shown that even in well-controlled laboratory experiments conducted with model colloid particles and uniform spherical collectors, the contribution of mechanisms such as deposition into a relatively deep secondary energy well or onto surface charge heterogeneities can cause significant deviation from classical CFT. These results have important implications for predictions of colloidal and microbial transport because the mechanisms identified are common to colloidal interactions in natural and engineered aquatic systems.

Glossary

A	Hamaker constant
A_S	porosity-dependent parameter of Happel's model
C	fluid-phase particle concentration
C_0	bulk (influent) particle concentration
d_c	diameter of spherical collector
k	particle deposition rate coefficient
k_B	Boltzmann constant, 1.3805×10^{-23} J/K
k_{fav}	deposition rate coefficient for deposition under *favorable* conditions
L	packed length of porous medium
N_A	attraction number
N_{dep}	total number of particles deposited during first phase of column experiment
N_G	gravity number
N_{Pe}	Peclet number
N_R	aspect ratio
N_{vdW}	van der Waals number
S	retained particle concentration
T	absolute temperature
t	time
U	approach (superficial) velocity of fluid
v	interstitial particle velocity
x	distance along column length

Greek Symbols

α	attachment (collision) efficiency, $\alpha = \eta/\eta_0$
α_{BTC}	attachment efficiency determined from particle breakthrough curve
α_{SLOPE}	attachment efficiency calculated from slope of retained particle profile
ϵ	porosity of a porous medium
$\Phi_{2^\circ min}$	depth of secondary energy minimum
Φ_{max}	height of energy barrier
η	single-collector removal efficiency; $\eta = \alpha \times \eta_0$
η_0	single-collector contact efficiency
μ	absolute viscosity of fluid
ρ	density of fluid
ρ_p	density of particle

Abbreviations

CFT	colloid filtration theory
DLVO	Derjaguin−Landau−Verwey−Overbeek
EDL	electrostatic double layer
VDW	van der Waals

Acknowledgment. The authors acknowledge the support of the U.S. Environmental Protection Agency (Award CR-82901001-0) and the Natural Sciences and Engineering Research Council of Canada (NSERC) for a graduate student fellowship to N.T.

LA048102G